High-Throughput Fabrication of Photoconductors with High Detectivity, Photosensitivity, and Bandwidth

Wendong Xing,[†] Sheng-Chin Kung,[†] Wytze E. van der Veer,[†] Wenbo Yan,[†] Talin Ayvazian,[†] Jung Yun Kim,[†] and Reginald M. Penner[†,‡,*]

[†]Department of Chemistry, University of California, Irvine, California 92697-2025, United States and [‡]Department of Chemical Engineering and Materials Science, University of California, Irvine, California 92697-2700, United States

ABSTRACT

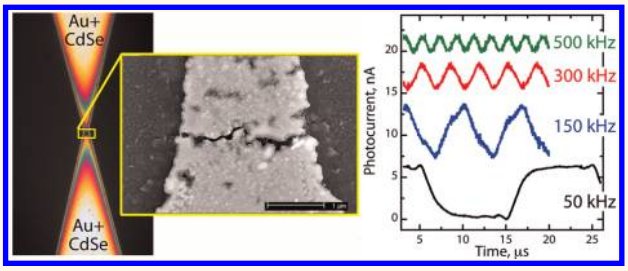

Nanocrystalline cadmium selenide (*nc*-CdSe) was electrodeposited within a sub-50 nm gold nanogap, prepared by feedback-controlled electromigration, to form a photoconductive metal−semiconductor−metal nanojunction. Both gap formation and electrodeposition were rapid and automated. The electrodeposited *nc*-CdSe was stoichiometric, single cubic phase with a mean grain diameter of ~7 nm. Optical absorption, photoluminescence, and the spectral photoconductivity response of the *nc*-CdSe were all dominated by band-edge transitions. The photoconductivity of these *nc*-CdSe-filled gold nanogaps was characterized by a detectivity of 6.9×10^{10} Jones and a photosensitivity of 500. These devices also demonstrated a maximum photoconductive gain of ~45 and response and recovery times below 2 μs, corresponding to a 3 dB bandwidth of at least 175 kHz.

KEYWORDS: electrodeposition · nanogap · electromigration · photodetector · cadmium selenide

An important attribute of photoconductors is their ability to produce gain in excess of 1.0, that is, the generation of more than one electron in an external circuit for each absorbed photon. In the absence of exotic effects like avalanche carrier multiplication[1] or multiple exciton generation,[2] photodiodes have a gain of ≤ 1.0.[3] The photoconductive gain, G, can be defined in terms of the free carrier lifetime, τ, and the transit time for carriers traveling between the two electrical contacts, τ_{tr}:[4]

$$G = \frac{\tau}{\tau_{tr}} \quad (1)$$

For nanowire photoconductors, G can be enormous because the proximity of photoexcited electrons and/or holes to nanowire surfaces facilitates carrier trapping which impedes recombination and increases τ. For example, Wang and co-workers[5] reported $G = 10^8$ for a single ZnO nanowire, a value that compares favorably with a photomultiplier tube (PMT),[3] but the time dependence of the photocurrent, $I_{photo}(t)$, in the dark is given by[4]

$$I_{photo}(t) = I_{photo,0}\exp\left(\frac{-t}{\tau}\right) \quad (2)$$

so while carrier trapping at nanowire surfaces increases both τ and G, it prolongs photocurrent recovery, thereby reducing the 3 dB bandwidth, f_{3dB}, over which the photoconductor can operate:[4]

$$f_{3dB} = \frac{1}{2\pi\tau} \quad (3)$$

The same ZnO nanowire that produced $G = 10^8$ had response and recovery times exceeding 50 s,[5] much slower than a PMT. Direct gap materials other than ZnO have a lower propensity to trap carriers, and nanowires of these materials (*e.g.*, CdSe, PbS, *etc.*) are, in general, capable of more rapid responses (Table 1), but it has been appreciated for many years that the fabrication of photoconductors that are *both* highly sensitive to light and respond and recover rapidly to light exposure is challenging.[4,6]

To break the stranglehold of the gain bandwidth product, the device geometry can be altered to focus attention on τ_{tr} instead of τ in eq 1 as a means to increase G.

* Address correspondence to rmpenner@uci.edu.

Received for review April 9, 2012 and accepted May 4, 2012.

Published online
10.1021/nn301567c

TABLE 1. Summary of Metal Chalcogenide-Based Photodetector Performance

material[a]	3 dB bandwidth (Hz)	detectivity[b] (Jones)	responsivity[c] (A/W)	photosensitivity $(I_{light} - I_{dark})/I_{dark}$	ref
PbS QD	18	1.80×10^{13}	1.00×10^{3}		28
PbS QD	3×10^{6}	1.00×10^{11}	2.25×10^{-1}		29
CdSe QD	50×10^{3}	1.0×10^{7}	1.80×10^{-3}	100	30
CdSe QD	0.1×10^{9}		5.70×10^{-6}		31
CdSe/ZnS QD	125×10^{3}	7.06×10^{7}	5.88×10^{-3}	7	8
CdSe NR	23×10^{3}		2.40×10^{2}	100	32
CdSe NR	350		2.40×10^{3}	2.33	25
CdSe NW	0.5		200	40	33
CdSe NW	44×10^{3}	3.77×10^{9}	1.30×10^{-2}	20	14
CdSe NW	0.043	4.46×10^{10}	1.70	300	14
CdSe in NG	175×10^{3}	6.90×10^{10}	9.1–31[d]	500	this work

[a] Abbreviations: Jones = cm × $Hz^{1/2}$ × W^{-1}; QD = quantum dot; NW = nanowire; NR = nanoribbon; NG = nanogap. [b] Detectivity either obtained by measuring the responsivity and noise current spectral density or calculated based on shot noise dominated noise current, which gives an upper bound on the detectivity that may actually be achieved. [c] The responsivity, R, is $R = I_{photo}/P_{opt} = (\eta G \lambda(\mu m))/1.24$, where η is the quantum yield and λ is the wavelength of the incident radiation. [d] R is estimated from the data of Figure 4e.

The τ_{tr} depends upon the device channel length L, electric field E, and carrier mobility μ according to

$$\tau_{tr} = \frac{L}{\mu E} \quad (4)$$

Combining eqs 1 and 4 and considering that $E = V/L$ (where V is applied voltage), we can express G as

$$G = \frac{\tau \mu V}{L^2} \quad (5)$$

From eq 5, it is apparent that by shrinking L, and therefore τ_{tr}, G can be increased without adversely affecting the τ and f_{3dB}. Using this strategy, Kim *et al.*[7] achieved response and recovery times of 7–8 ms for ZnO nanocrystals assembled into ~60 nm gold nanogaps—among the fastest photoconductivity responses seen for that material. Sensitivity metrics, however, were not reported for these devices. Hegg *et al.*[8] assembled CdSe/ZnS core–shell QDs into ~50 nm gold gaps to obtain photoconductors characterized by a high specific detectivity, $D^* = 7.06 \times 10^7$ Jones and a bandwidth exceeding 125 kHz. These data begin to validate this as a useful strategy for simultaneously maximizing sensitivity and speed in nanostructure-based photoconductors. In spite of its advantages, this approach has two important disadvantages: (1) Nanogaps must generally be created using expensive, slow, nanofabrication tools such as electron beam lithography (EBL)[9] or focused ion beam (FIB) milling.[10] Even less convenient from a process standpoint is the creation of nanogaps using mechanical break junctions.[11,12] (2) The insertion of semiconductor nanocrystals into the nanogap is irreproducible, especially in terms of the quality of the metal–semiconductor contacts that are established during this process.[7,8]

We demonstrate here a high-throughput method for preparing metal nanogap-based photoconductive detectors that circumvents both of these problems. In our process, programmable electromigration is used to reproducibly prepare nanogaps in a gold bowtie structure while electrodeposition provides a means for inserting a nanocrystalline CdSe absorber within these nanogaps. The resulting devices exhibit an even higher sensitivity to light ($D^* > 10^{10}$ Jones) coupled with the capability to switch rapidly between high conductivity (illuminated) and low conductivity (dark) states ($f_{3dB} >$ 175 kHz). These metrics are achieved by simultaneously minimizing both τ and τ_{tr}. This was accomplished by using, as the absorber, nanocrystalline CdSe (*nc*-CdSe) that is characterized by a τ of <1 μs.[13,14] This *nc*-CdSe is formed within a nanogap having minimum dimensions in the $L = 1$–10 nm range, produced by using feedback-controlled electromigration to fracture a 1.0–2.0 μm wide gold bowtie structure. In more detail, our process (Figure 1a) involves the fabrication of a 40 nm thick gold film with bowtie shape using thermal evaporation (step 0), photolithography (steps 1 and 2), and chemical etching (step 3 and Figure 1b). Then a nanogap is formed using electromigration[15–17] using a LabVIEW programmed voltage algorithm with a feedback mechanism (step 4). A nanocrystalline cadmium selenide (*nc*-CdSe) film is then electrodeposited on top of this nanogap electrode, bridging across it (step 5). Magnified optical micrographs (Figure 1c,d) show the device before (c) and after (d) the electrodeposition of *nc*-CdSe. This process is high-throughput in the sense that it employs highly parallel photolithography to produce the gold bowtie, coupled with programmable air and solution-based processes to complete device fabrication. Slow and expensive serial nanofabrication methods such as EBL and FIB milling are not required.

RESULTS AND DISCUSSION

Nanogap Formation by Electromigration. The feedback-controlled electromigration process used here was originally developed to produce 1–5 nm breaks in

gold nanowires with typical lateral dimensions of 100 nm (w) × 20 nm (h).[16] However, we used exactly the same algorithm to produce nanogaps in gold bowtie structures having minimum lateral dimensions of 1.0 μm (w) and 40 nm (h) in this work. Typical applied voltage, E_{app}, and resistance *versus* time traces for the electromigration process (Figure 2a) show that the algorithm for nanogap formation causes a stepwise decrease in E_{app} by 0.05 V whenever the time rate of change of the resistance exceeds a critical value. As shown in the SEMs of typical nanogaps shown in Figure 2b–d, a distribution of gap widths from 1 to 100 nm is produced by this process, but sections of each nanogap have dimensions reproducibly in the 1–10 nm range. This process provides a more expedient alternative to mechanical break junctions,[11,12] focused ion beam (FIB) milling[10] and e-beam lithography (EBL),[9] as a means for forming such nanometer-scale metal gap structures.

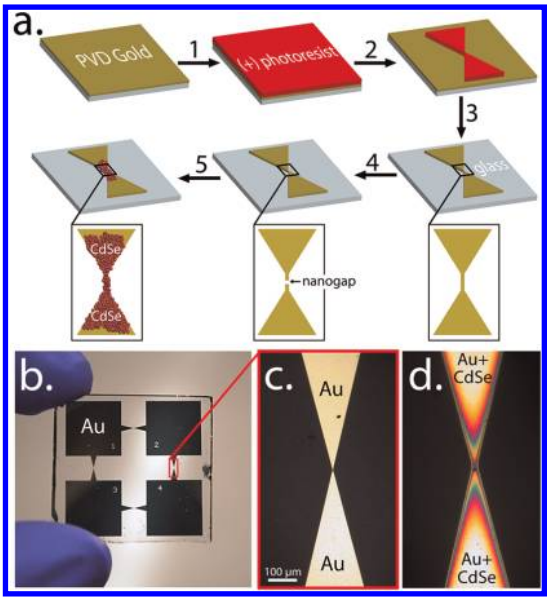

Figure 1. Fabrication of a Au–CdSe–Au nanogap photoconductor. (a) Schematic diagram showing the process flow for creating a nanogap and electrodeposition of *nc*-CdSe into it: (0) thermally evaporating a 1 nm/40 nm Cr/Au thin film on glass substrate, (1) spin-coating a (+) photoresist (PR) layer, (2) photopatterning the PR layer by a quartz contact mask with a 365 nm mercury UV lamp, (3) etching away the exposed Au and rinsing away the PR residue, (4) creating a nanogap by electromigration, (5) electrodepositing *nc*-CdSe into the nanogap. (b) Photograph of 1 in. × 1 in. glass slide with four Au bow–tie structures. (c) Zoomed in optical micrograph of an individual bow–tie structure. (d) Same device after *nc*-CdSe deposition with the color change coming from the variation in thickness of *nc*-CdSe.

Cadmium Selenide Synthesis by Electrodeposition. Electrodeposition of *nc*-CdSe onto nanogap structures was accomplished using both sides of the electromigrated gold bowtie as working electrodes, thereby ensuring that the electrodeposited *nc*-CdSe formed intimate electrical contacts across the nanogap. This electrical connectivity of the optically active layer with the gold electrode is not assured by introducing semiconductor nanocrystals into a nanogap either by drop casting[8] or by dielectrophoresis.[7] Previously,[13,14] we demonstrated that stoichiometric *nc*-CdSe could be electrodeposited using the scanning electrodeposition/stripping method first described by Sailor and co-workers.[18] However, in the present case, we found that the potential sweeps required by this method caused erosion of the gold nanogap, increasing its width. Instead, we prepared *nc*-CdSe

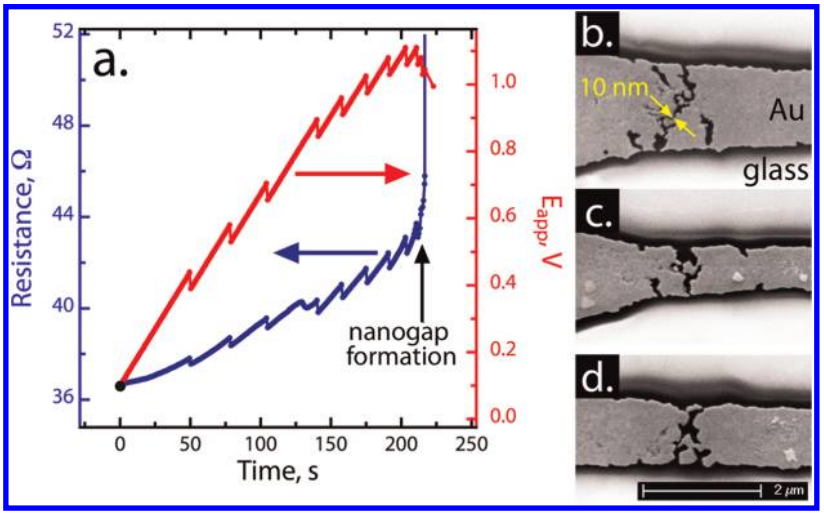

Figure 2. Nanogap formation by electromigration. (a) Applied voltage, E_{app} (red trace), and electrical resistance (blue trace) *versus* time for the formation of a nanogap by feedback-controlled electromigration. The algorithm for nanogap formation reduces E_{app} by 0.05 V when the time rate of change of the resistance exceeds a critical value. (b–d) Scanning electron micrographs of representative gold bowtie structures after electromigration, illustrating the diversity of nanogap structures that are obtained. Although a distribution of gap dimensions is obtained using this process, regions of these gaps are reproducibly in the 1–10 nm range. The white background in these images is caused by charging since these surfaces were not subjected to metal coating prior to SEM imaging.

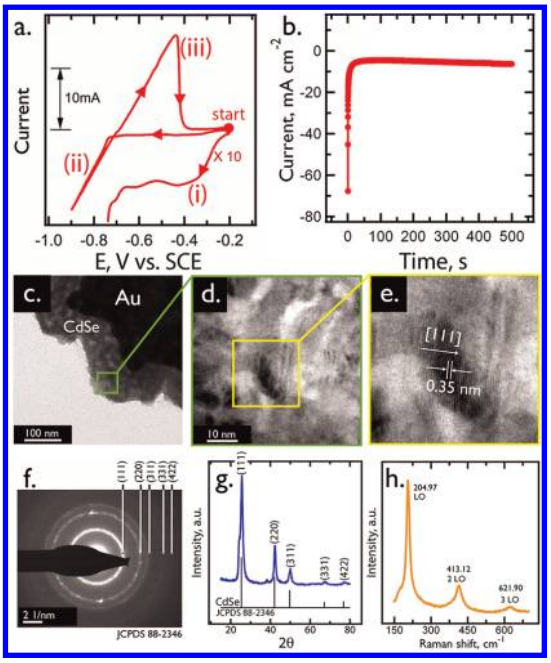

Figure 3. Electrodeposition and characterization of *nc*-CdSe. (a) Cyclic voltammetry (50 mV/s) of plating solution containing Cd^{2+} (0.30 M), SeO_3^{2-} (0.70 mM), pH = 1−2, adjusted by H_2SO_4. Peak (i) is magnified by a factor of 10 for clarity. Peak assignments are as follows: (i) $H_2SeO_3 + 4H^+ + 4e^- \rightarrow Se(s) + 3H_2O$; $Cd^{2+} + Se(s) + 2e^- \rightarrow CdSe(s)$; $Cd^{2+} + H_2SeO_3 + 4H^+ + 6e^- \rightarrow CdSe(s) + 3H_2O$. (ii) Process (i) and $Cd^{2+} + 2e^- \rightarrow Cd^0(s)$. (iii) $Cd^0(s) \rightarrow Cd^{2+} + 2e^-$. (b) Current *versus* deposition time for the electrodeposition of *nc*-CdSe at a potential of −0.6 V *vs* SCE. (c−e) Transmission electron micrographs at progressively higher magnification showing the nanocrystalline grain structure with a grain diameter of ≈7 nm. (f) Selected area electron diffraction (SAED) pattern indexed to cubic CdSe (JCPDS 88-2346). (g) Grazing-incidence X-ray diffraction (GIXRD) pattern acquired for a *nc*-CdSe thin film electrodeposited on a Au film on glass. Like the SAED pattern of (f), this GIXRD pattern is assigned to cubic CdSe (JCPDS 88-2346). (h) Raman spectrum of an electrodeposited *nc*-CdSe film on gold.

by potentiostatic electrodeposition from the same aqueous solution: 0.3 M $CdSO_4$, 0.7 mM SeO_2, and 0.25 M H_2SO_4, pH 1−2. The cyclic voltammetry of a gold electrode in this solution (Figure 3a) shows an onset for CdSe deposition near −0.25 V *vs* SCE. *NC*-CdSe was obtained using potentiostatic deposition at potentials in the range from −0.61 to −0.40 V, just negative of this onset. Deposition current *versus* time transients (Figure 3b) acquired at a potential of −0.60 V shows that rapid electrodeposition of CdSe onto a bare gold electrode decays within seconds as the surface becomes covered by *nc*-CdSe. After ∼50 s, a quasi-constant electrodeposition current was observed, consistent with activation control of the deposition process.[19] As-deposited *nc*-CdSe was used for structural, optical, and photoconductivity measurements without any subsequent thermal treatment. We found that *nc*-CdSe-coated gold bowtie structures were stable in ambient laboratory air, showing photoconductivity responses that were unchanged for periods of up to 1 month.

Cadmium Selenide Structural Characterization. Characterization of the electrodeposited CdSe layer using transmission electron microscopy (TEM, Figure 3c,d) reveals the crystallinity of the film with grain dimensions varying from 5 to 20 nm. At higher magnification (Figure 3e), lattice fringes spaced by 0.35 nm can be observed, corresponding to the *d* spacing along the [111] lattice direction of cubic CdSe. Selected area electron diffraction (SAED) analysis (Figure 3f) shows a diffuse ring pattern, as expected for polycrystalline material, with *d* spacings that are assignable to cubic CdSe (JCPDS 88-2346). This structural assignment is confirmed by grazing-incidence X-ray diffraction patterns (GIXRD, Figure 3g) that show well-resolved peaks for cubic CdSe and an absence of reflections corresponding to either elemental Cd or Se. Scherrer analyses[20] of the (111) or (220) reflections yield a mean grain diameter of ∼7 nm. Raman spectra (Figure 3h) are dominated by a strong mode at 205 cm^{-1} assignable to the longitudinal optical (LO) phonon mode[21] and 2−3 overtones of this mode, providing an indication of the high crystalline quality of these *nc*-CdSe films.

Optical and Photoconductivity Properties. A typical nanogap structure (Figure 4a,b) shown before (a) and after (b) CdSe electrodeposition (thickness ∼150 nm) demonstrates that the narrowest regions of the gap are bridged by *nc*-CdSe. The target thickness for the CdSe layer is somewhat less than $1/\alpha$ = 220 nm (absorption coefficient $\sim 4.5 \times 10^4\ cm^{-1}$),[22] ensuring that the incident light is fully absorbed by the material. The photoluminescence of the electrodeposited *nc*-CdSe (λ = 532 nm) is characterized by band-edge emission at 1.75 eV (Figure 4c, red trace). The absorption coefficient, α, as a function of photon energy, $h\nu$, can be interpreted in terms of the equation:[21]

$$\alpha = \frac{A(h\nu - E_g)^n}{h\nu} \qquad (6)$$

where E_g is the band gap of the absorber and A is a proportionality constant that depends upon the measurement geometry (Figure 4c, blue trace). For a direct transition, n = 1/2, whereas for an indirect transition, n = 2. Extrapolating the straight portion of the plot of $(\alpha \times h\nu)^2$ *versus* $h\nu$ (Figure 4c, inset) to the energy axis yields a band gap energy value of ∼1.76 eV. A photocurrent action spectrum (Figure 4d) shows an onset for photocurrent at 1.48 eV and a peak near 2.0 eV. The decay in photocurrent at higher photon energies above this peak, a ubiquitous feature of photocurrent action spectra including CdS[23,24] and CdSe[13,14,25] devices, is attributed to the enhanced absorption of high-energy photons in the near surface region

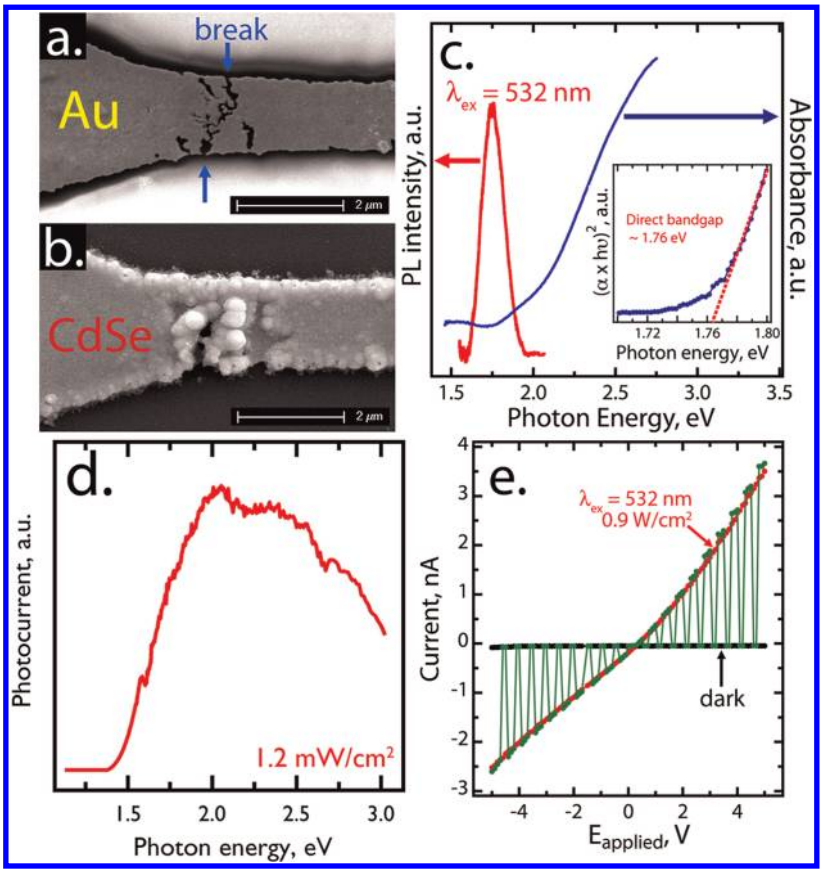

Figure 4. Optical and SEM device characterization. (a,b) Scanning electron micrographs of a nanogap formed by feedback-controlled electromigration (a) and the same nanogap after the electrodeposition of *nc*-CdSe (b). (c) Absorption spectrum for a *nc*-CdSe film (blue) and a photoluminescence spectrum for this film (red) acquired with excitation at 532 nm. The inset shows the plot of $(\alpha \times h\nu)^2$ against $h\nu$ (α is absorption coefficient). Extrapolating the linear region back to the energy axis provides an estimate of the direct band gap of ~1.76 eV. (d) Spectral response of the photocurrent for a bias of 1 V. Illumination was modulated at 135 Hz with a mean power of 1.2 mW/cm^2. (e) I_{dark} (black) and I_{light} (red) *versus* applied bias for a Au−CdSe−Au nanogap photoconductor. The green $I-V$ curve was acquired by switching between illumination (λ_{ex} = 532 nm, 0.9 W/cm^2) (red) and the dark state (black).

where the recombination rate is higher than in the bulk.[14,23] Collectively, these characterization data show that the wavelength dependence of this device closely approximates that expected for CdSe based upon a direct band gap of 1.75 eV. Current *versus* voltage curves for a typical nanogap structure in the dark (Figure 4e, black trace) and under illumination (532 nm, 0.9 W/cm^2, red trace) are consistent with a dc responsivity of 9.72 A/W in this case and a photosensitivity $(I_{light} - I_{dark})/I_{dark} \approx 500$.

The temporal properties of the photoconductivity response of *nc*-CdSe-filled gold nanogap structures were probed using modulated laser excitation at λ_{ex} = 532 nm.[14] The photocurrent *versus* time shows no amplitude dependence up to 20 kHz (Figure 5a). At higher modulation frequencies, the maximum photocurrent, I_{max}, begins to show attenuation at 150 kHz (Figure 5b). A plot of $((I_{max} - I_{min})/I_{max}$ %) *versus* the modulation frequency remains above 90% up to 150 kHz and then decreases beyond that threshold with f_{3dB} = 175 kHz, more than 1 order magnitude higher than for arrays of *nc*-CdSe nanowires (Figure 5c).[13] Moreover, the gain rolloff at 175 kHz response coincides with the bandwidth of a Keithley 428 current amplifier. Thus, f_{3dB} = 175 kHz comprises a lower limit for the bandwidth of *nc*-CdSe-filled gold nanogap structures.

The photocurrent amplitude is strongly dependent on the illumination power (Figure 5d), and this dependency is often described by a power law:[26]

$$I_{photo} \propto P_{optical}^{\gamma} \qquad (7)$$

The γ value fitted equals 0.86 $\pm$ 0.07 (Figure 5e). This sublinear behavior resembles that of photoconductive *nc*-CdSe nanowire arrays.[14] The canonical explanation is that traps are distributed with varying concentrations in the upper part of the band gap.[6] As the intensity of radiation increases, the quasi-Fermi level shifts toward the conduction band-edge and an increasing number of traps are converted into recombination centers.[6,27]

The specific detectivity, D^*, is a widely used figure of merit for photoconductors that is independent of the

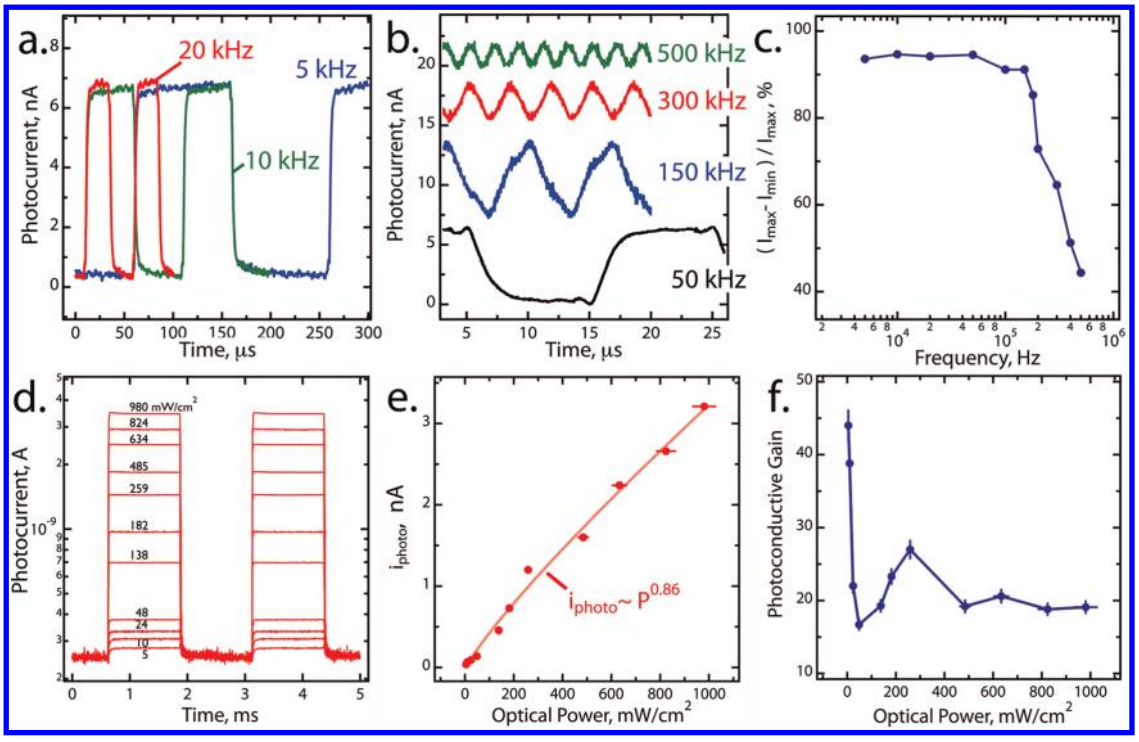

Figure 5. Photodetector performance. (a,b) Photocurrent *versus* time with illumination at 532 nm and 1.9 W/cm^2 modulated at frequencies of 5, 10, and 20 kHz (a) and 50, 150, 300, and 500 kHz (b). The bias applied is 5 V. Photocurrent traces in (b) are shifted along the current axis for clarity. (c) Normalized photocurrent ($(I_{max} - I_{min})/I_{max}$ %) *versus* the modulation frequency. (d) Photocurrent, measured at 400 Hz, as a function of optical power as indicated. (e) Photocurrent *versus* optical power, from the data shown in (d), also plotted is the best fit to the equation $I_{photo} \propto P_{optical}^{\gamma}$, $\gamma = 0.86 \pm 0.07$. (f) Estimated photoconductive gain, $G = (I_{photo}/P_{optical})(h\nu/q)$ *versus* optical power. It is assumed that 80% of the incident photons are absorbed. The active area is estimated to be 50 nm $\times$ 1 μm. Error bar is $\pm$5% of base value.

measurement system:[4]

$$D^* = \frac{R\sqrt{AB_n}}{I_n} \quad (8)$$

where R is the responsivity, A is the detector active area, B_n is the noise bandwidth, and I_n is the noise current.[4] If I_n is shot-noise-limited, $I_n = (2qIB_n)^{1/2}$, where I is total dark current.[4,8] Assuming an active area of 50 nm $\times$ 1 μm, D^* = 6.9 $\times$ 10^{10} Jones—a value competitive with the highest obtained in prior work (Table 1). G for these devices varies from 14 to 44 depending on the optical power (Figure 5f). These values are approximately a factor of 1000 higher than the G measured for arrays of *nc*-CdSe nanowires ($0.017 < G < 0.037$).[14] In that work, the electrically isolated nanowire length was 5 μm.[13,14] Since the *nc*-CdSe in these studies was prepared using an identical electrodeposition procedure, yielding an identical mean grain diameter (5−10 nm),[14] we attribute this dramatic increase in G to the reduction in L and τ_{tr} conferred by the nanogap geometry employed here.

SUMMARY

In summary, *nc*-CdSe-filled gold nanogaps are photoconductive detectors that simultaneously achieve high optical sensitivity and rapid response, characterized by high D^* (>10^{10} Jones), high R (>9 A/W), and high f_{3dB} (>175 kHz)—a combination that has not been demonstrated previously, to our knowledge (Table 1). These metrics are obtained by combining an absorber material, *nc*-CdSe, that has a τ in the microsecond range or below with a nanometer-scale channel. These devices may be rapidly and reproducibly fabricated using the new strategy described here, involving formation of a gold nanogap within a gold bowtie structure by feedback-controlled electromigration followed by electrodeposition of *nc*-CdSe directly in, and across, this nanogap.

EXPERIMENTAL SECTION

Chemicals and Materials. Cadmium sulfate ($3CdSO_4 \cdot 8H_2O$, 98+%), selenium oxide (SeO_2, 99.9+%), iodine (I_2, 99.8+%), and chromium etchant were used as received from Sigma-Aldrich. Sulfuric acid (ULTREX ultrapure) was purchased from J.T. Baker. Potassium iodide (KI, 99%) and acetone were used as received from Fisher (ACS Certified). Positive photoresist (Shipley, S1808) and developer (Shipley, MF-319) were purchased from Microchem Corporation. Gold pellets (5 N purity, ESPI Metals) and chromium powder (3 N purity, American Elements) were used for the evaporation of films.

Device Fabrication. As illustrated in Figure 1a, the process started from thermally evaporating a Cr/Au (1/40 nm) thin film

onto precleaned 1 in. × 1 in. squares of soda lime glass. Cr was used here as an adhesion layer. A positive photoresist (PR) layer (Shipley, S1808) was spin-coated (2500 rpm, 80 s), and a PR layer of ~800 nm thickness was formed after soft-baking (90 °C, 30 min). The PR was then patterned using a quartz contact mask in conjunction with a UV light source (365 nm, 500 W, ×2 s) equipped with a photolithographic alignment fixture (Newport, 83210-V). The exposed PR region was developed for 25 s (Shipley, MF-319) and rinsed with Millipore water (Milli-Q, ρ > 18 MΩ·cm). Exposed Au and Cr were removed by dipping in $KI/I_2/H_2O$ (4/2/40 g) solution for 10 s and standard Cr etchant (Aldrich) for 3 s, respectively, resulting in four bowtie structures with the narrow junction width of <2 μm. The PR layer was removed by rinsing with acetone. Then, electromigration was used to create a nanogap in the narrow junction, sequentially. After that, CdSe was electrodeposited into the nanogaps using fixed potential deposition, −0.6 V *vs* saturated calomel electrode (SCE), at room temperature. The plating solution was unstirred aqueous 0.30 M $CdSO_4$, 0.70 mM SeO_2, and 0.25 M H_2SO_4 at pH 1−2 (*Caution: both $CdSO_4$ and SeO_2 are highly toxic*). Electrodeposition was conducted in a one-compartment three-electrode electrochemical cell using a Gamry G300 potentiostat according to the procedure described in detail above. After CdSe electrodeposition, the sample was rinsed with Millipore water and air-dried. No post-electrodeposition thermal treatment was carried out.

This fabrication process was characterized by a high success rate of 15% overall: 30% for nanogap generation and 50% for *nc*-CdSe electrodeposition. The data reported in this paper were generated using six devices. These devices yielded stable photocurrent responses for several weeks in laboratory air.

Structural Characterization. Scanning electron microscopy (SEM) images were acquired using a Philips XL-30 FEG (field emission gun) SEM. Before CdSe electrodeposition, the nanogap was examined at an accelerating voltage of 5 keV without metal coating. After deposition, the sample was re-examined at 10 keV after plasma coating with Au/Pd to ameliorate charging.

Transmission electron microscopy (TEM) images and selected area electron diffraction (SAED) patterns were obtained using a Philips CM 20 TEM operating at 200 keV. TEM samples were prepared on top of a 10 nm thick Si_3N_4 membrane window centered on a 200 μm thick silicon frame (Norcada Inc.)

Grazing-incidence X-ray diffraction (GIXRD) patterns were obtained using a Rigaku Ultima III high-resolution X-ray diffractometer employing the parallel beam optics with a fixed incident angle of 0.3°. The X-ray generator was operated at 40 kV and 44 mA with Cu Kα irradiation. The JADE 7.0 X-ray pattern data processing software (Materials Data, Inc.) was used to analyze acquired patterns and estimate the respective grain diameter size.

Optical Properties. Absorption spectra were recorded from 850 to 450 nm using a UV−vis−NIR spectrophotometer (Perkin-Elmer, Lambda 950) equipped with tungsten halogen and deuterium light sources, double holographic grating monochromators, a photomultiplier and a Peltier-stabilized PbS detector, and a 60 mm integrating sphere (Lab Sphere, Inc.).

Raman and photoluminescence spectra were both acquired in a backscattering geometry using a Renishaw InVia Raman microscope with a 532 nm CW laser and a 2400 line/mm grating. The laser beam was focused onto the sample surface with an objective lens (N plan EPI, 50×/0.75), which yielded a beam spot of approximately 1 μm in diameter. An optical power of 50 mW was used in conjunction with an integration time of 30 s.

Photoconductivity. The spectral response of the photocurrent was measured using a home-built photocurrent spectrometer consisting of a 75 W xenon arc lamp (Oriel, 6255) coupled to a 1/4 m, F/3.9 monochromator (Oriel, MS-257) equipped with a 600 line/mm grating. The output of this light source was chopped at 135 Hz (Stanford Research Systems, SR-540) and focused onto the nanogap area. The resulting photocurrent was amplified (Keithley, 428-PROG) and detected using a dual-phase lock-in amplifier (EG&G, 5210). The photocurrent was normalized by the incident optical power (1.2 mW/cm^2 at 500 nm) measured using a digital power meter (Newport, 815) and a silicon photodiode (Newport, 818-SL). Samples were biased at 1.0 V.

The temporal response of photocurrent was measured for samples biased at 5.0 V and illuminated by a diode-pumped solid state, frequency-doubled Nd:VO_4 laser (532 nm, Sintec, ST-I-N-532). The output from this laser was modulated at frequencies up to 500 kHz using an acoustic optical modulator (AOM) system consisting of a fused silica crystal (Gooch & Housego, 35140-0.30-1.03-BR, rise time 15 ns), a RF AOM driver (Gooch & Housego, A35150) and a function generator (HP, 33120A). The modulated beam was focused onto the nanogaps by an objective lens (Mitutoyo Plan Apo, 20×/0.42), and its optical power was adjusted using a neutral density filter. The resulting photocurrent was amplified (Keithley, 428-PROG), detected, and averaged 16 383 times using a digital storage oscilloscope (Agilent, 54621A) triggered by the modulation signal from the function generator. All photoresponse measurements were carried out in ambient environment. Current *versus* voltage traces were measured using a sourcemeter (Keithley, 2400), and these data were recorded using a computer controlled by a LabVIEW program.

Conflict of Interest: The authors declare no competing financial interest.

Acknowledgment. The authors gratefully acknowledge the financial support of this work by the National Science Foundation (CHE-0956524) and University of California—Irvine, School of Physical Sciences Center for Solar Energy. The authors thank Prof. Matt Law for providing access to the Perkin-Elmer spectrophotometer used in this study. All electron microscopy was carried out in the Laboratory for Electron and X-ray Instrumentation (LEXI) at University of California, Irvine.

REFERENCES AND NOTES

1. Hayden, O.; Agarwal, R.; Lieber, C. Nanoscale Avalanche Photodiodes for Highly Sensitive and Spatially Resolved Photon Detection. *Nat. Mater.* **2006**, *5*, 352–356.
2. Sukhovatkin, V.; Hinds, S.; Brzozowski, L.; Sargent, E. H. Colloidal Quantum-Dot Photodetectors Exploiting Multiexciton Generation. *Science* **2009**, *324*, 1542–1544.
3. Sze, S. M.; Ng, K. K. *Physics of Semiconductor Devices*, 3rd ed.; Wiley-Interscience: Hoboken, NJ, 2007.
4. Rosencher, E.; Vinter, B. *Optoelectronics*; Cambridge University Press: Cambridge, UK, 2002.
5. Soci, C.; Zhang, A.; Xiang, B.; Dayeh, S. A.; Aplin, D. P. R.; Park, J.; Bao, X. Y.; Lo, Y. H.; Wang, D. ZnO Nanowire UV Photodetectors with High Internal Gain. *Nano Lett.* **2007**, *7*, 1003–1009.
6. Rose, A. *Concepts in Photoconductivity and Allied Problems*; Wiley-Interscience: New York, 1963; Vol. 19.
7. Seo, Y.-K.; Kumar, S.; Kim, G.-H. Photoconductivity Characteristics of ZnO Nanoparticles Assembled in Nanogap Electrodes for Portable Photodetector Applications. *Physica E* **2010**, *42*, 1163–1166.
8. Hegg, M. C.; Horning, M. P.; Baehr-Jones, T.; Hochberg, M.; Lin, L. Y. Nanogap Quantum Dot Photodetectors with High Sensitivity and Bandwidth. *Appl. Phys. Lett.* **2010**, *96*, 101118.
9. Fischer, P.; Chou, S. 10-nm Electron-Beam Lithography and Sub-50 nm Overlay Using a Modified Scanning Electron Microscope. *Appl. Phys. Lett.* **1993**, *62*, 2989–2991.
10. Menard, L. D.; Ramsey, J. M. Fabrication of Sub-5 nm Nanochannels in Insulating Substrates Using Focused Ion Beam Milling. *Nano Lett.* **2011**, *11*, 512–517.
11. Muller, C. J.; van Ruitenbeek, J. M.; de Jongh, L. J. Conductance and Supercurrent Discontinuities in Atomic-Scale Metallic Constrictions of Variable Width. *Phys. Rev. Lett.* **1992**, *69*, 140–143.
12. Reed, M.; Zhou, C.; Muller, C.; Burgin, T.; Tour, J. Conductance of a Molecular Junction. *Science* **1997**, *278*, 252–254.
13. Kung, S.-C.; van der Veer, W. E.; Yang, F.; Donavan, K. C.; Penner, R. M. 20 μs Photocurrent Response from Lithographically Patterned Nanocrystalline Cadmium Selenide Nanowires. *Nano Lett.* **2010**, *10*, 1481–1485.
14. Kung, S.-C.; Xing, W.; van der Veer, W. E.; Yang, F.; Donavan, K. C.; Cheng, M.; Hemminger, J. C.; Penner, R. M. Tunable Photoconduction Sensitivity and Bandwidth

for Lithographically Patterned Nanocrystalline Cadmium Selenide Nanowires. *ACS Nano* **2011**, *5*, 7627–7639.
15. Park, H.; Lim, A. K. L.; Alivisatos, A. P.; Park, J.; McEuen, P. L. Fabrication of Metallic Electrodes with Nanometer Separation by Electromigration. *Appl. Phys. Lett.* **1999**, *75*, 301–303.
16. Xiang, C.; Kim, J. Y.; Penner, R. M. Reconnectable Sub-5 nm Nanogaps in Ultralong Gold Nanowires. *Nano Lett.* **2009**, *9*, 2133–2138.
17. Xing, W.; Hu, J.; Kung, S.-C.; Donavan, K. C.; Yan, W.; Wu, R.; Penner, R. M. A Chemically-Responsive Nanojunction within a Silver Nanowire. *Nano Lett.* **2012**, *12*, 1729–1735.
18. Kressin, A.; Doan, V.; Klein, J.; Sailor, M. Synthesis of Stoichiometric Cadmium Selenide Films *via* Sequential Monolayer Electrodeposition. *Chem. Mater.* **1991**, *3*, 1015–1020.
19. Bard, A. J.; Faulkner, L. R. *Electrochemical Methods: Fundamentals and Aȧpplications*, 2nd ed.; Wiley: New York, 2001.
20. Patterson, A. L. The Scherrer Formula for X-ray Particle Size Determination. *Phys. Rev.* **1939**, *56*, 978–982.
21. Kale, R.; Sartale, S.; Chougule, B.; Lokhande, C. Growth and Characterization of Nanocrystalline CdSe Thin Films Deposited by the Successive Ionic Layer Adsorption and Reaction Method. *Semicond. Sci. Technol.* **2004**, *19*, 980–986.
22. Metin, H.; Erat, S.; Ari, M.; Bozoklu, M. Characterization of CdSe Films Prepared by Chemical Bath Deposition Method. *Optoelectron. Adv. Mater., Rapid Commun.* **2008**, *2*, 92–98.
23. Jie, J. S.; Zhang, W. J.; Jiang, Y.; Meng, X. M.; Li, Y. Q.; Lee, S. T. Photoconductive Characteristics of Single-Crystal CdS Nanoribbons. *Nano Lett.* **2006**, *6*, 1887–1892.
24. Li, Q.; Penner, R. Photoconductive Cadmium Sulfide Hemicylindrical Shell Nanowire Ensembles. *Nano Lett.* **2005**, *5*, 1720–1725.
25. Jiang, Y.; Zhang, W.; Jie, J.; Meng, X.; Fan, X.; Lee, S.-T. Photoresponse Properties of CdSe Single-Nanoribbon Photodetectors. *Adv. Funct. Mater.* **2007**, *17*, 1795–1800.
26. Kind, H.; Yan, H.; Messer, B.; Law, M.; Yang, P. Nanowire Ultraviolet Photodetectors and Optical Switches. *Adv. Mater.* **2002**, *14*, 158.
27. Joshi, N. V. *Photoconductivity: Art, Science, and Technology*; Marcel Dekker: New York, 1990.
28. Konstantatos, G.; Howard, I.; Fischer, A.; Hoogland, S.; Clifford, J.; Klem, E.; Levina, L.; Sargent, E. Ultrasensitive Solution-Cast Quantum Dot Photodetectors. *Nature* **2006**, *442*, 180–183.
29. Clifford, J. P.; Konstantatos, G.; Johnston, K. W.; Hoogland, S.; Levina, L.; Sargent, E. H. Fast, Sensitive and Spectrally Tuneable Colloidal Quantum-Dot Photodetectors. *Nat. Nanotechnol.* **2009**, *4*, 40–44.
30. Oertel, D.; Bawendi, M.; Arango, A.; Bulovic, V. Photodetectors Based on Treated CdSe Quantum-Dot Films. *Appl. Phys. Lett.* **2005**, *87*, 213505.
31. Pourret, A.; Guyot-Sionnest, P.; Elam, J. W. Atomic Layer Deposition of ZnO in Quantum Dot Thin Films. *Adv. Mater.* **2009**, *21*, 232–235.
32. Wu, P.; Dai, Y.; Sun, T.; Ye, Y.; Meng, H.; Fang, X.; Yu, B.; Dai, L. Impurity-Dependent Photoresponse Properties in Single CdSe Nanobelt Photodetectors. *ACS Appl. Mater. Interfaces* **2011**, *3*, 1859–1864.
33. Fan, Z.; Ho, J. C.; Jacobson, Z. A.; Razavi, H.; Javey, A. Large-Scale, Heterogeneous Integration of Nanowire Arrays for Image Sensor Circuitry. *Proc. Natl. Acad. Sci. U.S.A.* **2008**, *105*, 11066–11070.